

Motion Compensation in Short-scan CBCT Reconstructions for Dental Applications

Abdul Salam Rasmi Asraf Ali^{a,b}, Cristina Sarti^b, Claudio Landi^b, and Andrea Fusiello^a

^aDPIA, University of Udine, Italy

^bSee Through s.r.l., Brusaporto, Italy

ABSTRACT

Cone-beam computed tomography (CBCT) has revolutionized dental imaging by providing detailed three-dimensional representations of the maxillofacial region. However, its application in clinical practice is often impaired by patient movement during image acquisition, leading to severe image artifacts and compromised diagnostic accuracy. Cone beam CT system manufacturers have incorporated mechanical fixations to prevent patient movement, however, these fixtures lack complete rigidity and still permit some degree of movement. In clinical situations, short scan acquisitions are a common scenario where only a limited portion of the full 360° rotation is covered during the scan. A shorter scan has the advantage of a shorter exposure time and requires a device of smaller size which is very convenient due to space constraints in many dentist's clinics. This paper proposes a multi-stage approach to compensate for patient motion in short-scan CBCT reconstructions. In contrast to conventional iterative techniques that require multiple reconstructions during compensation, this approach requires only a few reconstructions computed with the Feldkamp-Davis-Kress (FDK) algorithm as the reference for compensation. Before the motion compensation stage, the reference volume undergoes regularization. The motion compensation is then accomplished by optimizing motion parameters through a regularized 3D-2D image registration process. The results show that the proposed motion compensation approach effectively reduces motion-induced artifacts in the final reconstruction.

Keywords: Motion compensation, dental CBCT, maxillofacial reconstruction, short-scan reconstruction

1. INTRODUCTION

Cone Beam Computed Tomography (CBCT) is a popular 3D imaging technique widely used in dentistry to provide detailed and accurate representations of dental structures. However, CBCT systems have a longer acquisition time compared to traditional CT scans, making them susceptible to artifacts due to patient motion during the imaging process. Research suggests that around 21-42% of *in vivo* CBCT examinations exhibit motion artifacts.¹ To prevent motion, manufacturers of CBCT systems use mechanical fixation devices such as head support and chin rest. However, these devices have some degree of flexibility to allow for patient comfort, so motion cannot be completely avoided. Existing solutions for motion compensation often involve complex algorithms that require multiple reconstructions of the complete set of projections, making the process time-consuming.²⁻⁴ Additionally, these approaches may suffer from inconsistencies resulting from data truncation and scatter, common issues encountered in CBCT imaging.⁵

In a previous paper,⁶ we introduced a method for compensating motion in a full 360° scan without the need for multiple iterations, effectively addressing the issues mentioned earlier. Expanding on the findings from our earlier work, this paper proposes a modification to our original approach to handle patient movements in short-scan reconstructions (covering 180° plus the fan angle). Short scans are generally preferred in clinical situations since only the minimum number of projections is collected to achieve good diagnostic quality. This, usually, means a shorter scan time and less dose for the patient. Also, CBCT devices that are designed for short-scan acquisitions have smaller footprints. However, despite these advantages, short-scan scenarios become more complex due to additional artifacts (referred to as short-scan artifacts) arising from the use of fewer projections. Motion can also significantly impact these scenarios due to the reduced number of projections. Although the reduction in projections is beneficial for faster scans and less patient movement, it can lead to increased artifacts in the presence of even minimal motion.

To address these challenges, our approach adopts a multi-stage strategy that still requires only a minimal number of reference reconstructions. Specifically, only two reference reconstructions are needed, and these are generated using the Feldkamp-Davis-Kress (FDK) algorithm,⁷ a well-established technique for reconstructing CBCT images. The primary goal of our method is to compensate for rigid motions that significantly degrade the reconstruction quality. A strong reduction of motion artifacts with a fast solution improves the final reconstructed image's quality and reliability, enabling the clinician to make a diagnosis without repeating the scan.

2. METHOD

The proposed method is illustrated in Figure 1. The process begins with an initial motion-affected reference reconstruction generated from the acquired projections. The knowledge of the acquisition geometry is crucial for this step and is encoded in the projection matrices containing information about the relative positions of the X-ray source, detector, and scanned object at each time step. The projection matrices are used for the initial reconstruction and to reproject the reconstructed volume. The synthetic projections obtained this way are registered with the original ones. Before reprojection, the reference reconstruction is regularized to increase the robustness of the registration (section 2.1). Registration is performed by optimizing the similarity score obtained using the cost function explained in section 2.2. Since the same reference reconstruction is used for all motion-affected projections, the optimizer can be run in parallel for multiple projections to save time. After the compensation process is completed, an intermediate reconstruction is performed using the estimated motion parameters. This intermediate reconstruction is used as the reference for the next stage of the compensation algorithm. This process can be repeated until the artifacts are eliminated. A final high-quality reconstruction is performed using the motion parameters estimated in the n^{th} stage.

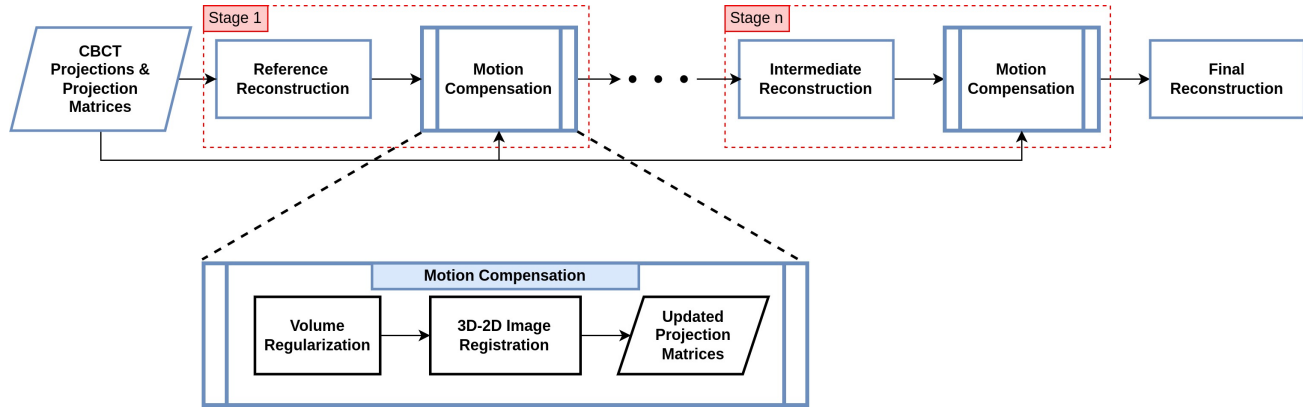
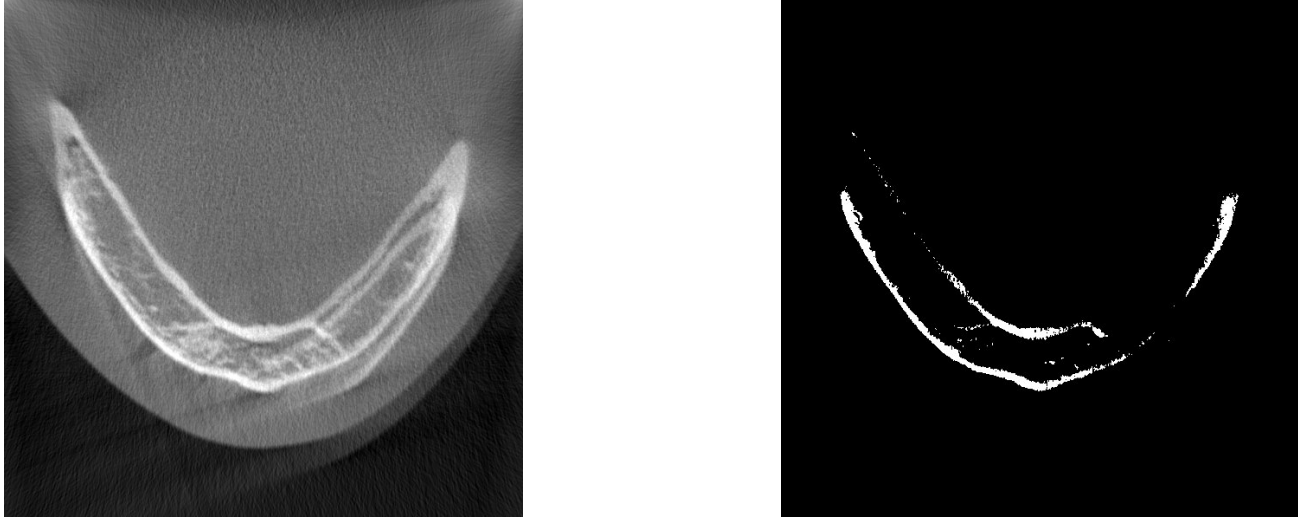


Figure 1: Pipeline of the proposed method

From our experiments, it turned out that after two stages the algorithm reached convergence. Further intermediate stages were not necessary since they did not provide any significant improvement in the final result.
Cristina maybe add here or somewhere else a graphic visualizing that after 2 steps the motion parameters do not change significantly

2.1 Regularization

Regularization of the reference reconstruction is necessary for three main reasons. Firstly, as shown in Figure 2a, motion artifacts like double contours or strong streaks affect the reference reconstruction leading to ambiguous overlapping structures during reprojection that are absent in real projections. Secondly, small structures in 2D projections are highly sensitive to motion, causing them to appear and disappear with each optimization step of the motion parameter modification. Thirdly, Poisson noise in the original projections further weakens low-contrast structures.



(a) Reference Reconstruction

(b) After Regularization

Figure 2: Regularization (The threshold is set to 1400 HU)

Consequently, reprojecting the reference reconstruction and registering them directly with original projections becomes challenging. To address this issue, we focus on identifying the most prominent structures, such as jawbones and teeth, by employing implicit regularization with a threshold-based segmentation of the reference reconstruction as shown in Figure 2b. During this particular step, our focus is on segmenting solely the hard tissues within the reference reconstruction. To accomplish this, we substitute any attenuation values exceeding a specific threshold with a constant value that closely approximates the average attenuation of the hard tissues. Any values below the threshold are discarded.

2.1.1 Threshold Selection

The selection of the threshold is based on the notable difference in attenuation coefficient values observed between soft tissues and hard tissues, as illustrated in Figure 3. In instances where less than one-third of the scan is affected by motion *Cristina Is this assumption realistic? What happens if more than one-third is affected? Add some short explanation perhaps referring to Spin-Neto's work*, motion artifacts, such as streaks and double contours, typically exhibit attenuation values lower than those of the jawbones and teeth. Therefore, we determined the threshold heuristically (see Figures 4 & 5) by identifying the attenuation value at which artifacts are effectively removed from the regularized volume. Choosing a threshold within this range (in our case, set at 1400 HU) efficiently eliminates the majority of artifacts found in the reference volume, as their attenuation coefficient values fall below the established threshold. The forward projection of the regularized reference volume results in a synthetic projection with high contrast, as shown in Figure 5d. This synthetic projection significantly contributes to achieving robust registration.

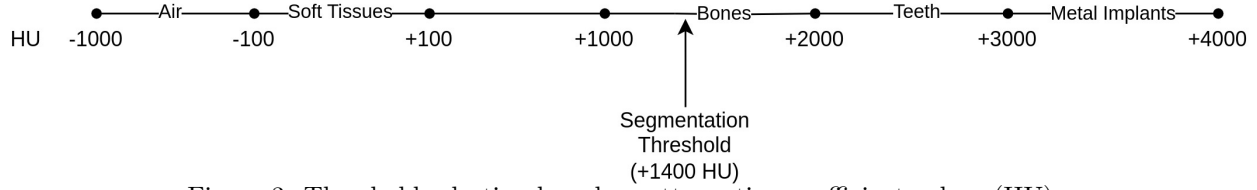


Figure 3: Threshold selection based on attenuation coefficient values (HU)

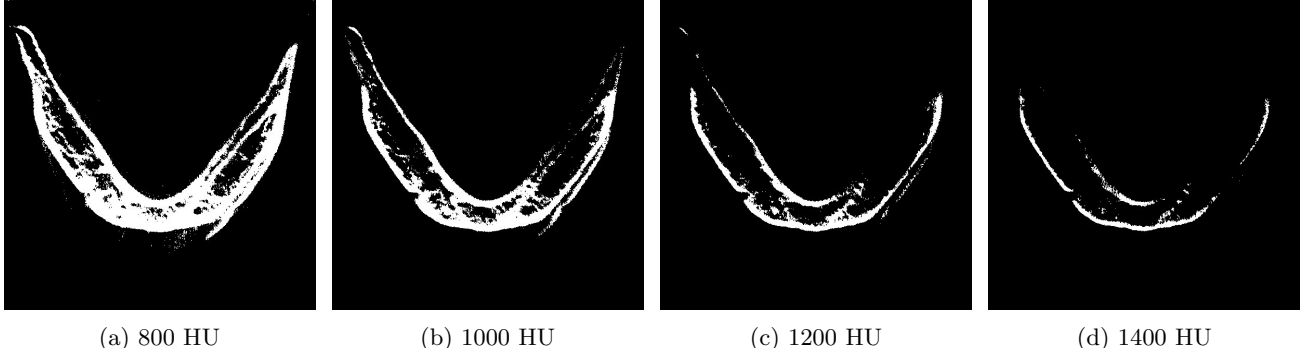


Figure 4: Regularization with different thresholds

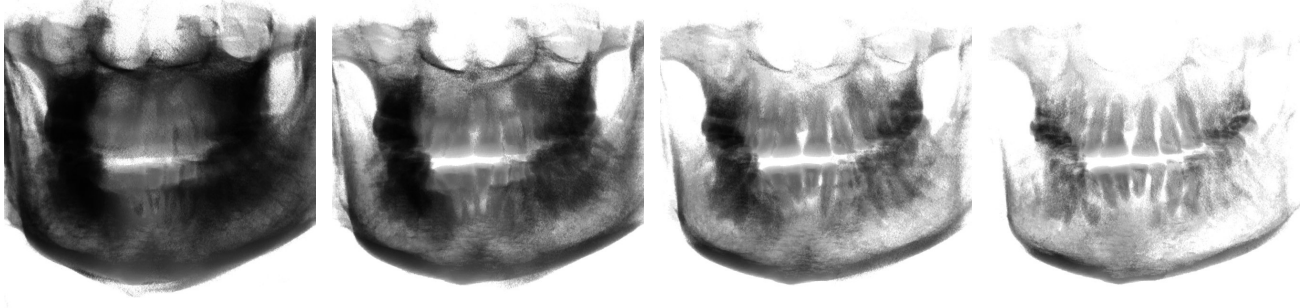


Figure 5: Forward Projection of regularized volumes for different thresholds

2.2 Similarity Cost Function

After the regularization step, the extracted strong edges are reprojected to generate the synthetic projections. We can therefore use a gradient strategy for image registration. We define our cost function based on Gradient Information, $G(r, a)$, which is the sum of the minima of gradient magnitudes computed for corresponding pixels in the synthetic image (r) and the actual image (a). This function is multiplied by a weighting function w and can be expressed as follows:

$$G(r, a) = \sum_{(\mathbf{x}, \mathbf{x}') \in (r \cap a)} w_{\mathbf{x}, \mathbf{x}'} \min(|\nabla \mathbf{x}|, |\nabla \mathbf{x}'|) \quad (1)$$

Where,

- \mathbf{x} and \mathbf{x}' refer to the corresponding sample points (pixels) in r and a , respectively.
- $|\nabla \mathbf{x}|$ and $|\nabla \mathbf{x}'|$ are the gradient magnitudes of \mathbf{x} and \mathbf{x}' , respectively.

The minima operator is applied to exclude strong extraneous gradients.⁸ The weighting function w in Equation 1 is the gradient orientation which is computed as the cosine of the angle between each corresponding gradient of r and a expressed as follows:

$$w_{\mathbf{x}, \mathbf{x}'} = \cos(\theta) = \frac{\nabla \mathbf{x} \cdot \nabla \mathbf{x}'}{|\nabla \mathbf{x}| |\nabla \mathbf{x}'|}. \quad (2)$$

3. EXPERIMENTAL RESULTS

3.1 Data

In this experiment, we used phantoms containing the skull and teeth of deceased patients, cast in a uniform plastic resin that approximates the X-ray attenuation of human soft tissue. Realistic motions were simulated using the strategy described in our previous paper.⁹ In this experiment, we assessed the algorithm's performance across different positions defined by the relative orientation of the detector to the patient's head. We simulated nodding motions in three distinct positions: first with the detector on the right side, followed by one with the detector in front, and finally, one with the detector on the left side of the patient's head. This experimental setup was designed to investigate the algorithm's limitations concerning the detector's position. We simulated three returning nodding motions, where the patient returns to the initial position, as illustrated in Figure 6. Additionally, we simulated three non-returning nodding motions, where the patient does not return to the initial pose after movement, as illustrated in Figure 7. These scenarios are challenging because non-returning motions create double contours in the reconstruction (Figure 12), affecting the majority of projections and complicating diagnosis. To evaluate the quality of the final reconstruction, we performed a motion-free short-scan reconstruction of 194° to serve as a ground truth for comparison.

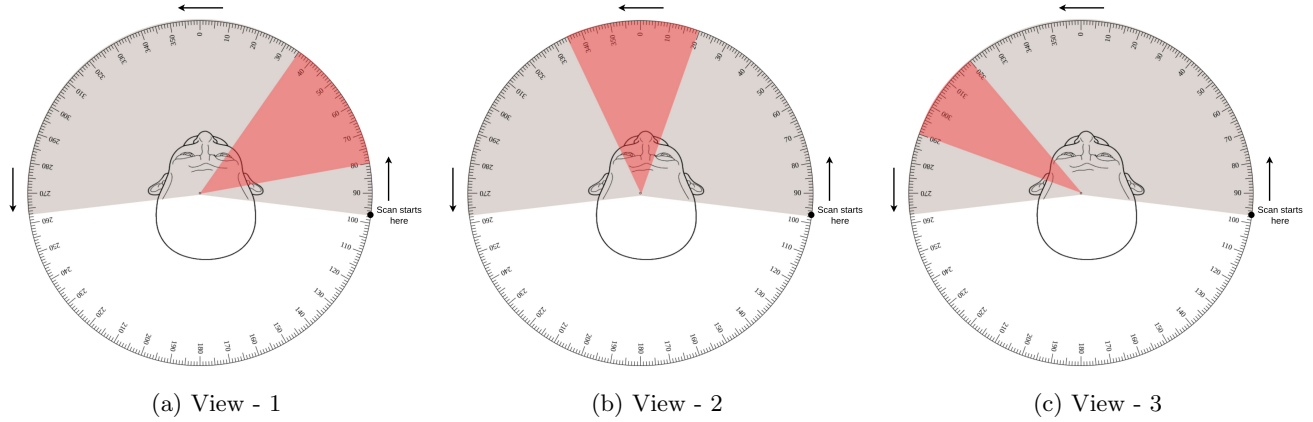


Figure 6: Illustration showing the motion-affected subset (red) and motion-free subset (gray) of projections in the short-scan angle for nodding motion (returning)

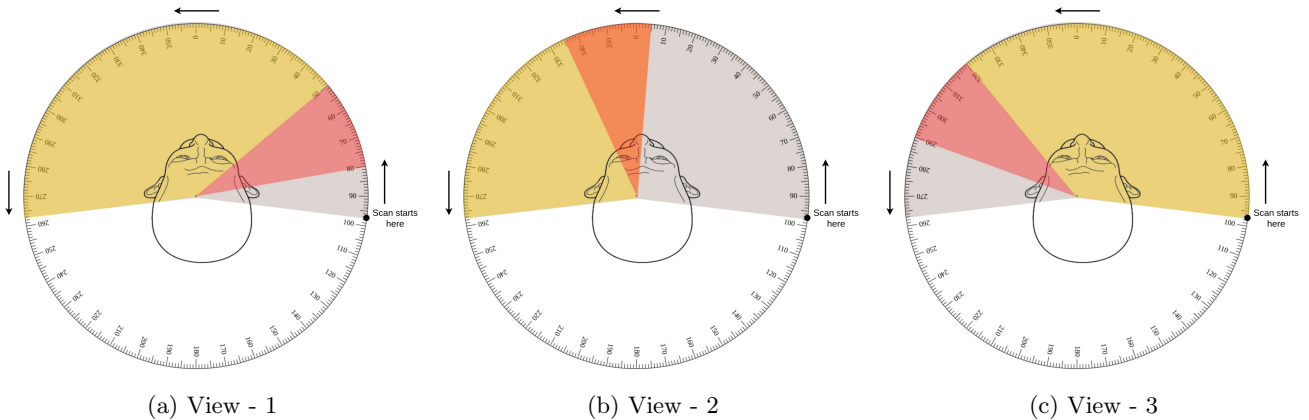


Figure 7: Illustration showing the motion-affected and motion-free subsets for nodding motion (non-returning). 'red' indicates patient movement, while 'gray' and 'yellow' signify instances where the patient remains stationary but in distinct poses.

3.2 Returning Motion Results

Figures 8, 9, and 10 present a comparison among the reconstructions affected by motion, motion-compensated reconstructions, and the ground truth for the three test cases of returning nodding motions mentioned above. In all three scenarios, the second stage of motion compensation notably reduced motion artifacts. It's important to highlight that although some minor artifacts are noticeable, crucial diagnostic structures remain free from motion artifacts and are clearly visible. The maximum duration of applied motion is 3 seconds, accounting for approximately one-fourth of the short-scan duration.

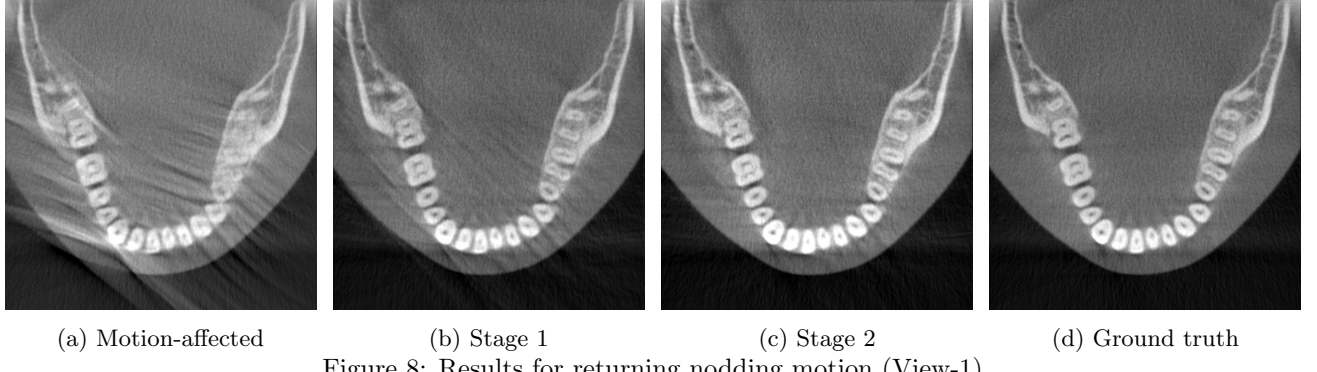


Figure 8: Results for returning nodding motion (View-1)

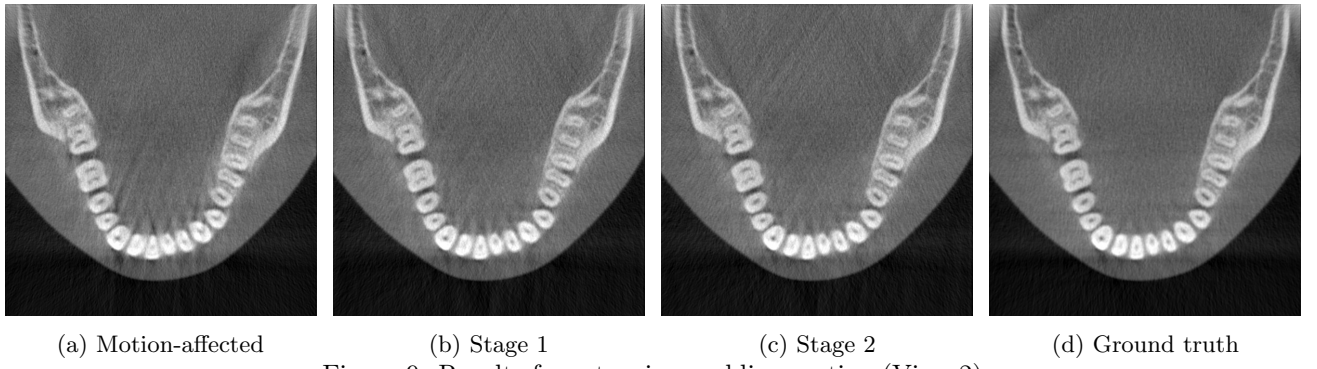


Figure 9: Results for returning nodding motion (View-2)

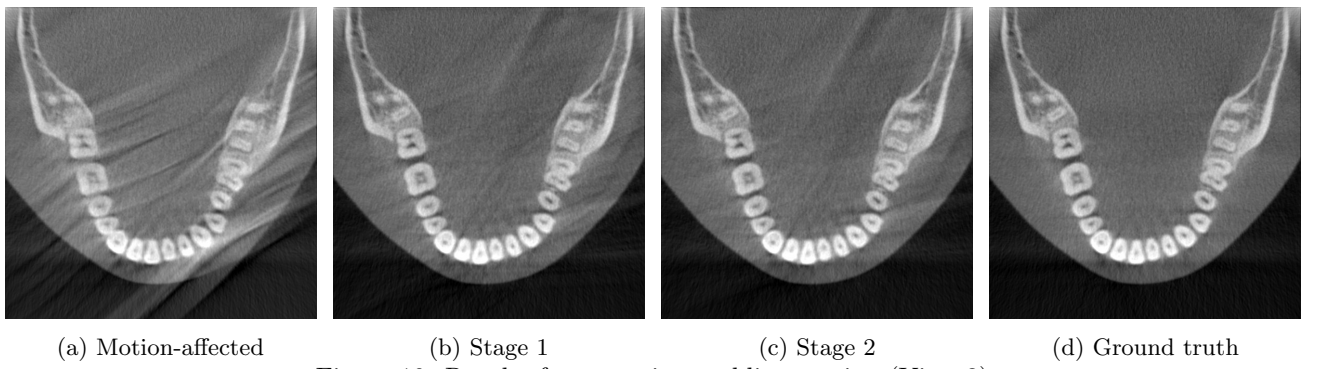


Figure 10: Results for returning nodding motion (View-3)

Table 1 provides a summary of the quantitative evaluations for the three tests of returning nodding motions. Notably, there is a substantial enhancement in View-1 and a slight improvement in View-3. However, in

View-2, the SSIM score decreases for the motion-compensated reconstruction. This discrepancy arises because the SSIM score is computed for the entire 3D volume, encompassing a significant portion of free space where diagnostic structures are absent. Nevertheless, despite this decrease in SSIM score, the clinical value of the motion-compensated image surpasses that of the motion-affected reconstruction.

Table 1: SSIM and RMSE values for nodding motions (returning) [MA = motion-affected, MC = motion-compensated]

View	SSIM (\uparrow)			RMSE ($\times 10^{-2}$) (\downarrow)		
	MA	MC	Diff %	MA	MC	Diff %
View - 1	0.783	0.826	+4.33	4.22	4.17	-0.05
View - 2	0.837	0.817	-1.98	2.49	2.47	-0.02
View - 3	0.825	0.835	+0.91	3.32	2.85	-0.47

3.3 Non-returning Motion

Figures 11, 12, and 13 present a comparison among reconstructions affected by motion, motion-compensated reconstructions, and the ground truth for the three instances of non-returning nodding motions outlined in Section 3.1. In the case of View-1, the motion compensation algorithm demonstrated strong performance, notably reducing motion artifacts. This success is because nearly three-fourths of the scan duration remained unaffected by motion. Consequently, the regularization technique effectively removed the minor artifacts present in the reference reconstruction. The SSIM and RMSE scores presented in Table 2 are consistent with the qualitative analysis, reflecting similar outcomes.

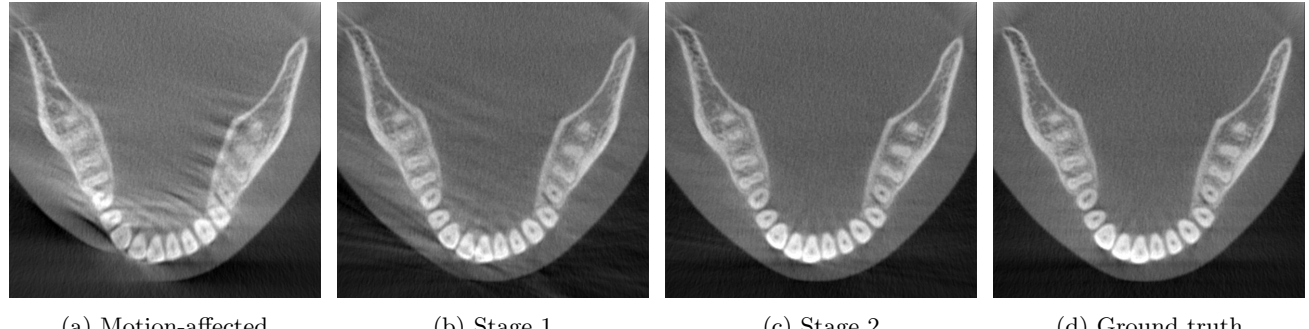
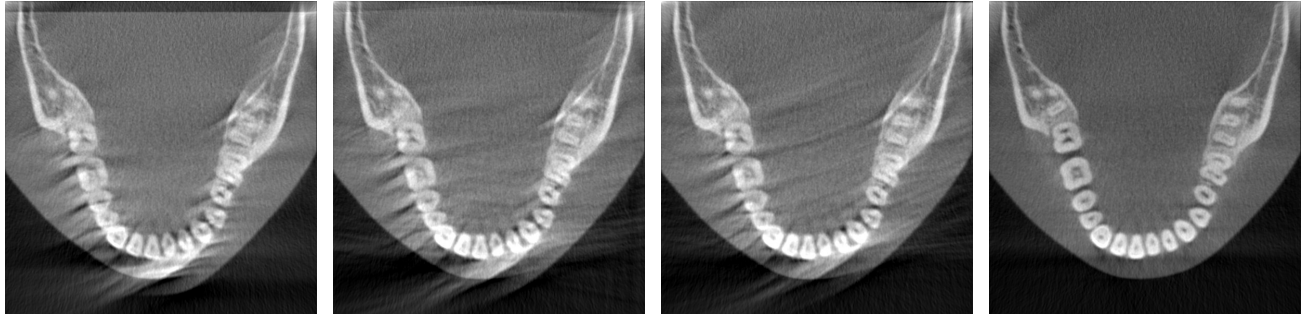


Figure 11: Results for non-returning nodding motion (View-1)



Figure 12: Results for non-returning nodding motion (View-2)



(a) Motion-affected

(b) Stage 1

(c) Stage 2

(d) Ground truth

Figure 13: Results for non-returning nodding motion (View-3)

However, in the remaining two scenarios (View-2 & View-3), despite the simulated patient movement being brief, the challenge arises from it being a non-returning motion. This poses challenges for the regularization technique, particularly when artifacts have higher attenuation values like those of bones and teeth (Figure 14). Consequently, the compensation algorithm struggled to effectively eliminate motion artifacts in these instances.



(a) Motion-affected

(b) Stage 1

Figure 14: Regularization results of non-returning nodding motion (View-2). The highlighted area indicates an artifact with a higher attenuation value that persists even after regularization.

Table 2: SSIM and RMSE values for nodding motions (non-returning) [MA = motion-affected, MC = motion-compensated]

View	SSIM (\uparrow)			RMSE ($\times 10^{-2}$) (\downarrow)		
	MA	MC	Diff %	MA	MC	Diff %
View - 1	0.743	0.833	+8.97	5.78	2.47	-3.31
View - 2	0.628	0.558	-7.02	7.53	8.26	+0.73
View - 3	0.726	0.750	+2.38	5.95	3.50	-2.45

4. CONCLUSION

Our approach introduces a novel method that proficiently compensates for motion artifacts in short-scan CBCT reconstructions. Through a multi-stage process and the application of a suitable regularization to the reference reconstructions, our method achieves high-quality results for cases where less than one-third of the scan is affected by patient motion. Compared to other reconstruction methods (e.g. iterative reconstruction approaches), the FDK reconstruction algorithm holds greater popularity in the clinical industry combining fast processing with a good diagnostic quality of the reconstructed volume. Consequently, employing the motion compensation approach with the FDK algorithm makes it an ideal choice for clinicians. However, when dealing with prolonged motion scenarios, such as non-returning motions, a modification to our current method seems to be essential to obtain artifact-free reconstructions. One viable modification involves integrating a partial angle motion compensation approach into our method, as suggested by Hahn et al.¹⁰ Furthermore, to assess the robustness of our proposed method across diverse scenarios, additional tests involving more complex motions and clinical data are essential.

ACKNOWLEDGMENTS

The authors thank Michele Antonelli, Ivan Tomba, Andrea Delmiglio, Lorenzo Arici from See Through s.r.l., and Prof. Giovanni Di Domenico from the University of Ferrara, Italy for providing the projection data and the reconstruction libraries.

REFERENCES

- [1] Spin-Neto, R., Matzen, L. H., Schropp, L., Gotfredsen, E., and Wenzel, A., “Factors affecting patient movement and re-exposure in cone beam computed tomography examination,” *Oral surgery, oral medicine, oral pathology and oral radiology* **119**(5), 572–578 (2015).
- [2] Maur, S., Stsepankou, D., and Hesser, J., “Cbct auto-calibration by contour registration,” in [*Medical Imaging 2019: Physics of Medical Imaging*], **10948**, 413–421, SPIE (2019).
- [3] Sun, T., Jacobs, R., Pauwels, R., Tijskens, E., Fulton, R., and Nuysts, J., “A motion correction approach for oral and maxillofacial cone-beam ct imaging,” *Physics in Medicine & Biology* **66**(12), 125008 (2021).
- [4] Birklein, L., Niebler, S., Schömer, E., Brylka, R., Schwancke, U., and Schulze, R., “Motion correction for separate mandibular and cranial movements in cone beam ct reconstructions,” *Medical physics* **50**(6), 3511–3525 (2023).
- [5] Würfl, T., Hoffmann, M., Aichert, A., Maier, A. K., Maaß, N., and Dennerlein, F., “Calibration-free beam hardening reduction in x-ray cbct using the epipolar consistency condition and physical constraints,” *Medical physics* **46**(12), e810–e822 (2019).
- [6] Asraf Ali, A. S. R., Sarti, C., and Landi, C., “Compensation for patient movements in cbct imaging for dental applications,” in [*Image Analysis and Processing – ICIAP 2023*], Foresti, G. L., Fusello, A., and Hancock, E., eds., 540–551, Springer Nature Switzerland, Cham (2023).
- [7] Feldkamp, L. A., Davis, L. C., and Kress, J. W., “Practical cone-beam algorithm,” *Josa a* **1**(6), 612–619 (1984).
- [8] De Silva, T., Uneri, A., Ketcha, M., Reaungamornrat, S., Kleinszig, G., Vogt, S., Aygun, N., Lo, S., Wolinsky, J., and Siewerdsen, J., “3d–2d image registration for target localization in spine surgery: investigation of similarity metrics providing robustness to content mismatch,” *Physics in Medicine & Biology* **61**(8), 3009 (2016).
- [9] Asraf Ali, A. S. R., Fusello, A., Landi, C., Sarti, C., and Siswadi, A. A. P., “Motion artifacts detection in short-scan dental cbct reconstructions,” *arXiv preprint arXiv:2304.10154* (2023).
- [10] Hahn, J., Bruder, H., Rohkohl, C., Allmendinger, T., Stierstorfer, K., Flohr, T., and Kachelrieß, M., “Motion compensation in the region of the coronary arteries based on partial angle reconstructions from short-scan ct data,” *Medical physics* **44**(11), 5795–5813 (2017).